Analysis of a Composite Double Cantilever Beam with Stitched Reinforcements Under Mixed Mode Loading : Formulation (I)

Insik Jang*
Department of Mechano-Informatics and Design Engineering, Hongik University, 300 Jochiwon-eup, Yonki-gun, Chungnam-do 339-701, Korea
Bhavani V. Sankar
Department of Mechanical and Aerospace Engineering, University of Florida, P.O.Box 116250 Gainesville, FL 32611-6250, U.S.A

Several methods for improving the interlaminar strength and fracture toughness of composite materials are developed. Through-the-thickness stitching is considered one of the most common ways to prevent delamination. Stitching significantly increases the Mode I fracture toughness and moderately improves the Mode II fracture toughness. An analytical model has been developed for simulating the behavior of stitched double cantilever beam specimen under various loading conditions. For z-directional load and moment about the y-axis the numerical solutions are compared with the exact solutions. The derived formulation shows good accuracy when the relative error of displacement and rotation between numerical and exact solution were calculated. Thus we can use the present model with confidence in analyzing other problems involving stitched beams.

Key Words : Composite Double Cantilever Beam, Stitched Reinforcement, Mixed Mode Loading, Analytical Modelling

Nomenclature

A_s: Cross-sectional area of the stitch yarn
A_t: Cross-sectional area of beam
b : Beam width
c : The length of bridging zone
E : Equivalent Young's modulus of beam
E_s: Young's modulus of the stitch material
G : Equivalent shear modulus of beam
h_t : Height of top beam
I_t : Moment of inertia of beam
k : Spring constant of stitch
M_t: y-directional moment at top beam
N : Number of stitches per unit area
P_t : x-directional load at top beam
t_n : z-directional traction by stitch
t_s : x-directional traction by stitch
u_t : x-directional displacement
V_t: z-directional load at top beam
w_t: z-directional y-displacement
ψ_t : Rotation about y-axis

The subscript t indicates the top beam property and b the bottom beam property.

* Corresponding Author,
E-mail : isjang@hongik.ac.kr
TEL : +82-41-860-2608; **FAX** : +82-41-866-6152
Department of Mechano-Informatics and Design Engineering, Hongik University, 300 Jochiwon-eup, Yonki-gun, Chungnam-do 339-701, Korea. (Manuscript **Received** July 1, 2004; **Revised** December 20, 2004)

1. Introduction

Composite materials are utilized increasingly in industry because of high strength with relatively low weight. Especially, graphite-epoxy laminated composites have very high stiffness and strength to weight ratios, which make them very attractive in structural applications. The orientation of the fibers has significant effect on the in-plane properties of these materials. The strength in the thickness direction, however, is limited by

the matrix material, and is typically about 5 to 10% of the strength in the fiber direction. Therefore, these materials suffer from poor interlaminar properties, and easily delaminate.

Several methods for improving the interlaminar strength and fracture toughness of these materials include 3D weaving, Z-pinning and stitching. Translaminar reinforcement can be provided by inserting pins in the thickness direction (z-pinning) of the laminate or by stitching the layers with suitable yarns before resin impregnation. Through-the-thickness stitching is considered one of the most common ways to prevent delamination. Sankar and Sharma (1995) report that stitching significantly increases the Mode I fracture toughness and moderately improves the Mode II fracture toughness. In practical applications it is very rare to encounter pure Mode I or Mode II loading conditions, since it is typical to have a combination of the two modes. Ridards and Korjakin (1998) used the traditional mixed mode setup to test the fracture toughness of unstitched laminated composites. Reeder and Crews (1992) proposed a new mixed-mode bending method for delamination testing. This test allows a wide range of ratios of Mode I and Mode II and has several advantages over the traditional methods. Chen, Ifju and Sankar (2001) developed new methodology and testing apparatus for double cantilever beam test for stitched composite laminates. Rugg, Cox and Massabo (2002) investigated the mixed mode delamination behavior of carbon-epoxy laminates by using two different test specimens. Other fracture mechanics from cracks subjected to mixed-mode loading can be found. Choi and Chai (2002, in Korea) investigated interfacial crack initiation and propagation using biaxial loading device for various mixed modes. Song and Lee (2003, in Korea) analyzed the propagation behavior of fatigue cracks of cold rolled stainless steel under mixed -mode conditions. Although there are several approaches for testing of stitched composites, not much work has been done in developing analytical models. Sankar and Dharmapuri (1998) proposed analytical method for stitched DCB (double cantilever beam) with Mode I loading condition. They found a closed form solution for the problem of beam on elastic foundation and utilized the model to simulate the DCB test and subsequent crack propagation. Chen, Sankar and Ifju (2003) proposed a new methodology for testing mixed mode DCB specimens. The developed apparatus is very efficient to apply the mixed mode load. They compared the results of experiments and finite element analysis as well. In this study, an analytical approach is proposed for stitched DCB under mixed mode loading conditions. The related differential equations are derived and solved for several loading conditions. The numerical results are compared with the exact solutions and the accuracy of the numerical solution is discussed.

2. Analytical Model of Stitched Double Cantilever Beam

The problem to be solved is depicted in Fig. 1. The Timoshenko beam theory is used to determine the deflections and rotations in the stitched beam.

It is assumed that DCB has different heights at top and bottom parts. The applied load is represented as F_x, x-directional load, and F_z, z-directional load, respectively. The length from the end of beam to the first stitch is defined as a. The bridging zone is a region in which there exist unbroken stitches in the crack opening. The length of bridging zone is defined as c in Fig. 1.

The shape of stretched stitch is depicted in detail in Fig. 2 when mixed mode load is applied. The points A and B are coincident before

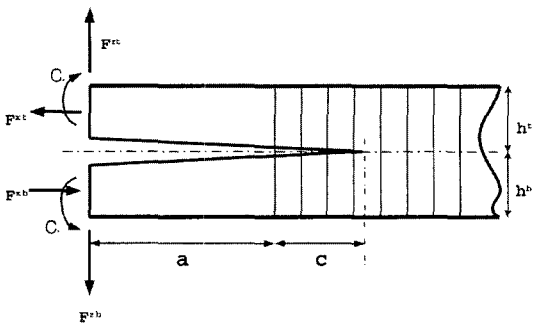

Fig. 1 Typical stitched double cantilever beam

loading. u and w represent x-directional displacement and z-directional displacement, respectively. Therefore, the length of a stitch increases by AB.

In the present study the stitch is considered as a spring with spring constant k, which is calculated as

$$k=\frac{2NA_sE_s}{h_t+h_b} \tag{1}$$

The factor 2 appears in Eq. (1) to account for the two bobbin yarns that constitute one through the thickness stitch. Traction due to the stitches in the x and z-directions are computed as

$$\begin{aligned} t_n&=k\Delta w=k(w_t-w_b)\\ t_s&=k\Delta u=k(u_t-u_b) \end{aligned} \tag{2}$$

The equilibrium equations involving, the longitudinal force, shear force and bending moment are described using the displacements and spring constant of the stitch as follows:

$$\frac{dP_t}{dx}=t_sb=bk(u_t-u_b) \tag{3}$$

$$\frac{dV_t}{dx}=t_nb=bk(w_t-w_b) \tag{4}$$

$$\frac{dM_t}{dx}=V_t-\frac{h_t}{2}bk(u_t-u_b) \tag{5}$$

From the laminate constitutive equations we can obtain the following relations between force resultants and displacements:

$$P_t=A_tE\frac{du_t}{dx} \tag{6}$$

$$M_t=I_tE\frac{d\psi_t}{dx} \tag{7}$$

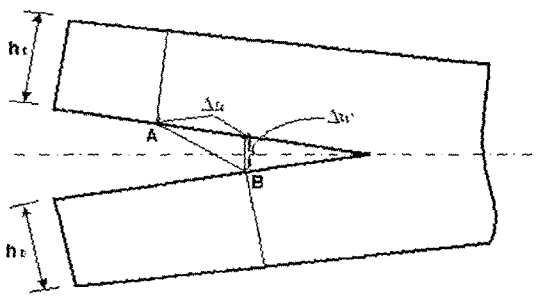

Fig. 2 Deformation of a stitch under mixed mode load

$$V_t=A_tG\left(\frac{dw_t}{dx}+\psi_t\right) \tag{8}$$

Combining (3)-(8) results in governing equations for the top part of the stitched DCB take the form,

$$A_tE\frac{d^2u_t}{dx^2}-bk(u_t-u_b)=0 \tag{9}$$

$$EI_t\frac{d^2\psi_t}{dx^2}-GA_t\psi_t-GA_t\frac{dw_t}{dx}+\frac{h_t}{2}bk(u_t-u_b)=0 \tag{10}$$

$$GA_t\frac{d\psi_t}{dx}+GA_t\frac{d^2w_t}{dx^2}-bk(w_t-w_b)=0 \tag{11}$$

Let us define three stiffness constants for the convenience of representation of equations.

$$\frac{A_tE}{b}=B_t:\text{ axial stiffness}$$

$$\frac{EI_t}{b}=D_t:\text{ flexural stiffness}$$

$$\frac{A_tG}{b}=Q_t:\text{ shear stiffness}$$

Then the governing equations (9)-(11), can be rewritten using the newly defined stiffness constants.

$$B_t\frac{d^2u_t}{dx^2}-k(u_t-u_b)=0 \tag{12}$$

$$D_t\frac{d^2\psi_t}{dx^2}-Q_t\psi_t-Q_t\frac{dw_t}{dx}+\frac{h_t}{2}k(u_t-u_b)=0 \tag{13}$$

$$Q_t\frac{d\psi_t}{dx}+Q_t\frac{d^2w_t}{dx^2}-k(w_t-w_b)=0 \tag{14}$$

Similar equations for the bottom beam can be derived as follows.

$$B_b\frac{d^2u_b}{dx^2}+k(u_t-u_b)=0 \tag{15}$$

$$D_b\frac{d^2\psi_b}{dx^2}-Q_b\psi_b-Q_b\frac{dw_b}{dx}+\frac{h_b}{2}k(u_t-u_b)=0 \tag{16}$$

$$Q_b\frac{d\psi_t}{dx}+Q_b\frac{d^2w_b}{dx^2}+k(w_t-w_b)=0 \tag{17}$$

It may be noted that the tractions exerted by the stitches on the top and bottom are equal and opposite, and hence the sign reversal in terms containing the stiffness constant kin the equations for the bottom beam. Boundary conditions at the ends of the beam are as follows.

At $x=0$ one can apply, in general, an axial force, a transverse force and a couple, Therefore, the force boundary conditions are:

$$P_t=A_tE\frac{du_t}{dx}=F_{xt},\ P_b=A_bE\frac{du_b}{dx}=F_{xb}$$
$$M_t=I_tE\frac{d\psi_t}{dx}=C_t,\ M_b=I_bE\frac{d\psi_b}{dx}=C_b \tag{18}$$
$$V_t=A_tG\left(\frac{dw_t}{dx}+\psi_t\right)=F_{zt}$$
$$V_b=A_bG\left(\frac{dw_b}{dx}+\psi_b\right)=F_{zb}$$

At $x=c$ the rigid end boundary conditions are given by:

$$w_t=w_b=0,\ \psi_t=\psi_b=0,\ u_t=u_b=0 \tag{19}$$

3. Solution Procedure for the Governing Equations

The longitudinal displacements u_t and u_b can be found by solving equations (12) and (15) simultaneously. Rearranging (12) and (15) and eliminating u_b will result in a 4th order differential equation in u_t as

$$\frac{d^4u_t}{dx^4}-\left(\frac{1}{B_t}+\frac{1}{B_b}\right)ku_t''=0 \tag{20}$$

Let us assume solution of the form:

$$u_t=ce^{\lambda x} \tag{21}$$

By substituting the solutions from equation (21) into the governing equation (20) we obtain the solution:

$$u_t=c_1+c_2x+c_3e^{\lambda_1 x}+c_4e^{\lambda_2 x} \tag{22}$$

where

$$\lambda_1=\sqrt{\left(\frac{1}{B_t}+\frac{1}{B_b}\right)k},\ \lambda_2=-\sqrt{\left(\frac{1}{B_t}+\frac{1}{B_b}\right)k}$$

and from the relationship between u_t and u_b in equation (12)

$$u_b=c_1+c_2x+c_3\left(1-\frac{B_t}{k}\lambda_1^2\right)e^{\lambda_1 x}+c_4\left(1-\frac{B_t}{k}\lambda_2^2\right)e^{\lambda_{21}x} \tag{23}$$

After applying the boundary conditions, the simultaneous equations for the unknown constants can be represented in a matrix form

$$\begin{bmatrix} 0 & 1 & \lambda_1 & \lambda_2 \\ 0 & 1 & \lambda_1\left(1-\frac{B_t}{k}\lambda_1^2\right) & \lambda_2\left(1-\frac{B_t}{k}\lambda_2^2\right) \\ 1 & c & e^{\lambda_1 c} & e^{\lambda_2 c} \\ 1 & c & \left(1-\frac{B_t}{k}\lambda_1^2\right)e^{\lambda_1 c} & \left(1-\frac{B_t}{k}\lambda_2^2\right)e^{\lambda_1 c} \end{bmatrix}\begin{Bmatrix} c_1 \\ c_2 \\ c_3 \\ c_4 \end{Bmatrix}=\begin{Bmatrix} \frac{P_t}{bB_t} \\ \frac{P_b}{bB_b} \\ 0 \\ 0 \end{Bmatrix} \tag{24}$$

The x-directional displacement (22) and (23) can be obtained by solving the above simultaneous equations.

By differentiating (14) and (17) with respect to x and eliminating w_t and w_b, we can obtain the coupled differential equations for ψ_t and ψ_b

$$D_t\psi_t''''-k\left(\frac{D_t}{Q_t}\psi_t''-\frac{D_b}{Q_b}\psi_b''\right)+k(\psi_t-\psi_b)$$
$$=\frac{k^2}{2}\left(\frac{h_t}{Q_t}-\frac{h_b}{Q_b}\right)(u_t-u_b)-\frac{h_t}{2}k(u_t''-u_b'') \tag{25}$$

$$D_{bt}\psi_b''''+k\left(\frac{D_t}{Q_t}\psi_t''-\frac{D_b}{Q_b}\psi_b''\right)-k(\psi_t-\psi_b)$$
$$=-\frac{k^2}{2}\left(\frac{h_t}{Q_t}-\frac{h_b}{Q_b}\right)(u_t-u_b)-\frac{h_t}{2}k(u_t''-u_b'') \tag{26}$$

Let us assume the solutions of the equations (25) and (26) as

$$\psi_t=pe^{\alpha x},\ \psi_b=qe^{\alpha x} \tag{27}$$

If we substitute the equation (27) into equations (25) and (26) we obtain the following simultaneous equation for finding p and q

$$\begin{bmatrix} D_t\alpha^4-k\frac{D_t}{Q_t}\alpha^2+k & k\frac{D_b}{Q_b}\alpha^2-k \\ k\frac{D_t}{Q_t}\alpha^2-k & D_b\alpha^4-k\frac{D_b}{Q_b}\alpha^2+k \end{bmatrix}\begin{Bmatrix} p \\ q \end{Bmatrix}=\begin{Bmatrix} R_t \\ R_b \end{Bmatrix} \tag{28}$$

where R_t and R_b represent non-homogeneous terms. For the specific α_i, the ratio of coefficients p_i and q_i is computed as

$$r_i=\frac{q_i}{p_i}=-\frac{D_t\alpha_i^4-k\frac{D_t}{Q_t}\alpha_i^2+k}{k\left(\frac{D_b}{Q_b}\alpha_i^2-1\right)} \tag{29}$$

To make the problem simple let us assume that the cross sections of bottom and upper beams are identical. Then, the stiffness constants become $D_t=D_b=D$, $Q_t=Q_b=Q$.

For the homogenous solutions we can obtain the roots of characteristic equation :

$$\alpha_{1,2,3,4}=0 \tag{30}$$

$$\alpha_{5,6,7,8}=\pm\sqrt{\frac{k}{Q}\pm\sqrt{\left(\frac{k}{Q}\right)^2-\frac{2k}{D}}} \tag{31}$$

Homogeneous solutions for ψ_t and ψ_b can be expressed as :

$$\psi_{th}=\sum_{i=1}^{4}p_i x^{i-1}+\sum_{k=5}^{8}p_i e^{a_i x} \tag{32}$$

$$\psi_{bh}=\sum_{i=1}^{4}r_i p_i x^{i-1}+\sum_{k=5}^{8}r_i p_i e^{a_i x} \tag{33}$$

The general solutions for ψ_t and ψ_b become

$$\begin{aligned}\psi_t&=\psi_{th}+g_3e^{\lambda_1 x}+g_4e^{\lambda_2 x}\\&=\sum_{i=1}^{4}p_i x^{i-1}+\sum_{i=5}^{8}p_i e^{a_i x}+g_3e^{\lambda_1 x}+g_4e^{\lambda_2 x}\\\psi_b&=\psi_{bh}+h_3e^{\lambda_1 x}+h_4e^{\lambda_2 x}\\&=\sum_{i=1}^{4}r_i p_i x^{i-1}+\sum_{i=5}^{8}r_i p_i e^{a_i x}+h_3e^{\lambda_1 x}+h_4e^{\lambda_2 x}\end{aligned} \tag{34}$$

where the coefficients g and h can be obtained by applying the particular parts in equation (28). The constants g_3 and h_3 can be calculated using equations (35) and (36) shown below, which are derived from (25) and (26) by substituting the particular solutions, $\psi_{tp_1}=g_3e^{\lambda_1 x}$, $\psi_{bp}{}^1=h_3e^{\lambda_1 x}$, and the particular functions, $u_t=c_3e^{\lambda_1 x}$, $u_b=c_3\left(1-\frac{B_t}{k}\lambda_1^2\right)e^{\lambda_1 x}$.

$$\left(D\lambda_1^4-\frac{D}{Q}k\lambda_1^2+k\right)g_3+\left(\frac{D}{Q}k\lambda_1^2-k\right)h_3=-\frac{hB}{2}c_3\lambda_1^4 \tag{35}$$

$$\left(\frac{D}{Q}k\lambda_1^2-k\right)g_3+\left(D\lambda_1^4-\frac{D}{Q}k\lambda_1^2+k\right)h_3=-\frac{hB}{2}c_3\lambda_1^4 \tag{36}$$

Similar procedures may be used to obtain g_4 and h_4.

We need eight boundary conditions to determine p_i, $i=1, \cdots, 8$. They correspond to (18) and (19) at the two ends of the top and bottom beams, The expression for w_t and w_b that include unknowns b_i, $i=1, \cdots, 8$ can be obtained by substituting (34) into equations (13) and (16).

$$\begin{aligned}w_t=&\left(\frac{2D}{Q}p_3-p_1\right)x+\frac{1}{2}\left(\frac{6D}{Q}p_4-p_2\right)x^2\\&-\frac{1}{3}p_3x^3-\frac{1}{4}p_4x^4+\sum_{i=5}^{8}\left(\frac{D}{Q}a_i^2-1\right)\frac{p_i}{a_i}e^{a_i x}\\&+\left(\frac{D}{Q}\lambda_1^2-1\right)\frac{g_3}{\lambda_1}e^{\lambda_1 x}+\left(\frac{D}{Q}\lambda_2^2-1\right)\frac{g_4}{\lambda_2}e^{\lambda_2 x}\\&+\frac{1}{2}\frac{h}{Q}B(c_3\lambda_1e^{\lambda_1 x}+c_4\lambda_2e^{\lambda_2 x})\end{aligned} \tag{37}$$

$$\begin{aligned}w_b=&\left(\frac{2D}{Q}p_3-p_1\right)x+\frac{1}{2}\left(\frac{6D}{Q}p_4-p_2\right)x^2\\&-\frac{1}{3}p_3x^3-\frac{1}{4}p_4x^4+\sum_{i=5}^{8}\left(\frac{D}{Q}a_i^2-1\right)\frac{r_ip_i}{a_i}e^{a_i x}\\&+\left(\frac{D}{Q}\lambda_1^2-1\right)\frac{h_3}{\lambda_1}e^{\lambda_1 x}+\left(\frac{D}{Q}\lambda_2^2-1\right)\frac{h_4}{\lambda_2}e^{\lambda_2 x}\\&+\frac{1}{2}\frac{h}{Q}B(c_3\lambda_1e^{\lambda_1 x}+c_4\lambda_2e^{\lambda_2 x})\end{aligned} \tag{38}$$

By applying the eight boundary conditions related to rotation and transverse displacements we obtain a set of linear equations in the coefficients P_i which are given in Appendix I. Once the coefficients are determined, the solution of the problem depicted in Fig. 2 is obtained. Deriving the expressions for the deflection curve, stitch elongation and energy release rate at the crack tip, calculating shear force and bending moment resultants, at any cross section are matter of straightforward computation and are discussed in the following section.

4. Numerical Results and Discussion

Graphite/epoxy is selected as the beam material and Kevlar® is the stitch material for the present analysis. The beam is assumed to be 7 inches long and 0.71 inch wide, stitched with 1600 denier Kevlar yarn with two yarns in each stitch. The stitch density is $4\times\frac{1}{5}''$ means that there are 20 stitches per square inch, where the pitch is 1/4 inch and the spacing between two adjacent stitch rows is 1/5 inch. For simplicity we consider that the depth of top beam is equal to that of bottom beam. The mechanical properties of the beam and stitch materials are summarized in Tables 1 and 2, respectively.

To validate the formulation derived here we compare the displacements calculated from this

procedure with the exact solution (Young, 1989). The bridging zone of stitched DCB under loads is considered as a finite length beam on elastic foundation subjected to transverse forces and bending moment. The stiffness of elastic foundation is equivalent to the spring constant calculated in equation (1). The exact solutions are expressed in analytical form, and are shown in Appendix II.

The example problem is to analyze a part of DCB with stitch reinforcement under z-directional load or moment about y-axis, which are depicted in Fig. 1. We confine the analyzed region within bridging zone of the beam. The length of bridging zone, which is denoted by c, is taken as 1 inch.

Numerical and analytical results of z-direction displacement are shown in Fig. 3 for applied z-directional loads, which are $F_{zb}=5000$ N and $F_{zt}=-5000$ N. It is very difficult to differentiate the numerical result from the analytical one in Fig. 3 because the two results have almost same value. We introduce the relative error, the difference between numerical solution and the exact one divided by the largest displacement, to evaluate the accuracy of the numerical result. It can be noted from Fig. 4 that the present method is very accurate with a maximum error of 1.4%.

The rotation of beam due to the applied z-directional force is shown in Fig. 5. The relative error, rotation difference divided by the largest rotation, shows high accuracy (max. 0.7%) as well in Fig.6.

In Fig. 7 through 10, displacements, rotation and related relative error for applied moments

Table 1 Mechanical properties of beam

E_1(psi)	E_2(psi)	ν_{12}	G_{12}(psi)	G_{13}(psi)	G_{23}(psi)
15.04×10^6	1.6×10^6	0.34	0.8×10^6	0.8×10^6	0.52×10^6

Table 2 Mechanical properties of stitch

Material	Specific gravity	Tensile strength (GPa)	Elastic modulus (GPa)
Kevlar	1.44	2.8	130

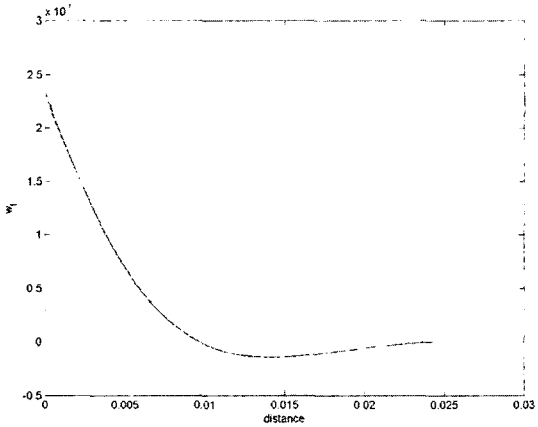

Fig. 3 Comparison of z-direction displacement for applied load (solid : numerical, dotted : analytical)

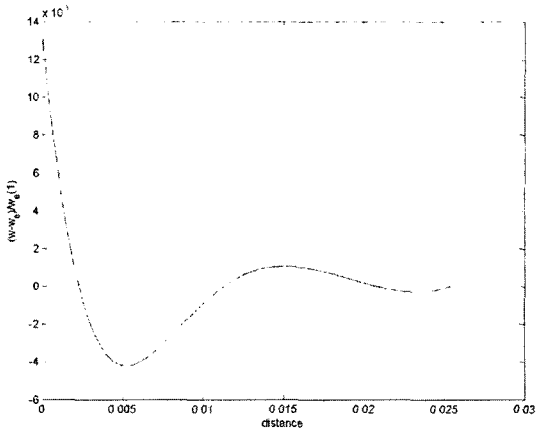

Fig. 4 Relative z-direction displacement error for applied load

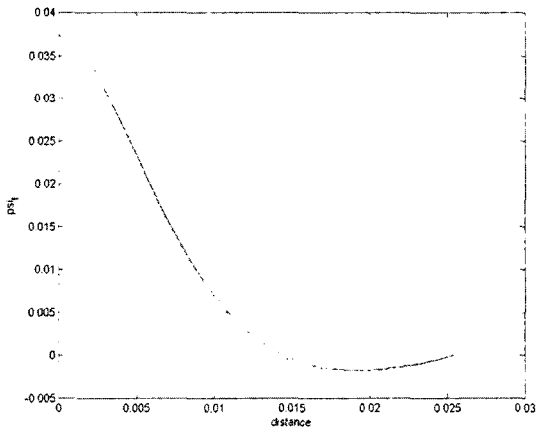

Fig. 5 Comparison of rotation for applied load (solid : numerical, dotted : analytical)

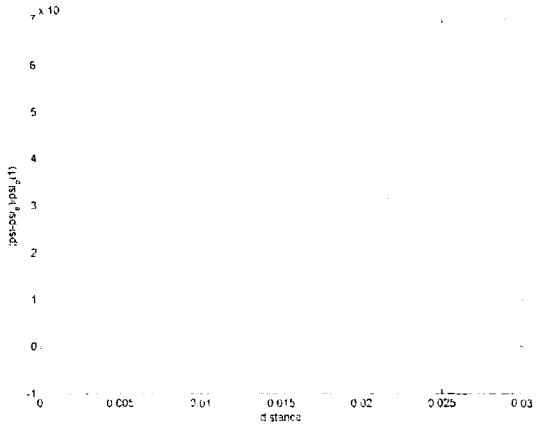

Fig. 6 Relative rotation error for applied load

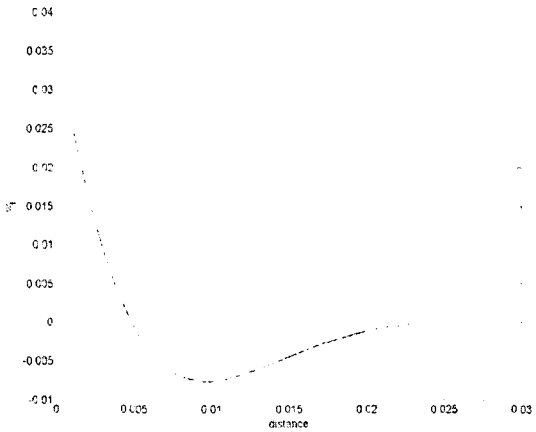

Fig. 7 Comparison of z-direction displacement for applied moment (solid : numerical, dotted : analytical)

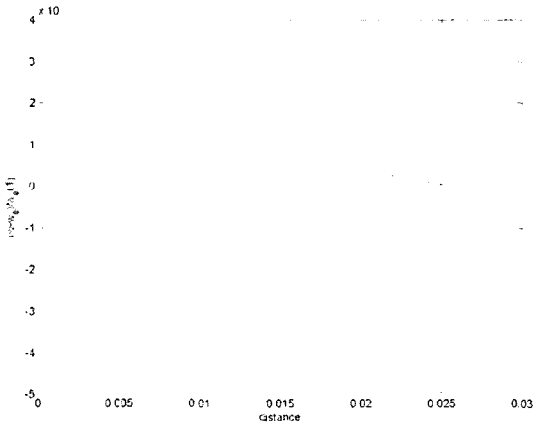

Fig. 8 Relative z-direction displacement error for applied moment

are shown. The applied moments are $C_t = -5000$ N·m and $C_b = 5000$ N·m. From accuracy point of view these results represent almost same trend as the cases of applied transverse load.

From the results above, the present formulation for stitched beams is accurate enough to be utilized to calculate the displacements for various load conditions.

We may classify the type of load in the DCB by the fracture Mode. Mode I case is wherein the applied loads are symmetrical about the plane of delamination and the crack tip is under Mode I fracture condition. In this mode the applied load is in the positive z-direction on the upper beam and negative z-direction on the lower beam as

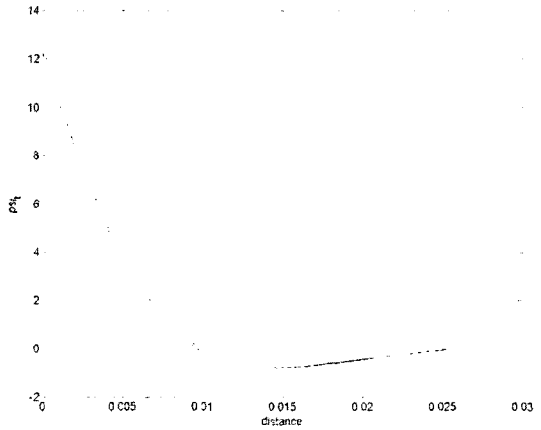

Fig. 9 Comparison of rotation for applied moment (solid : numerical, dotted : analytical)

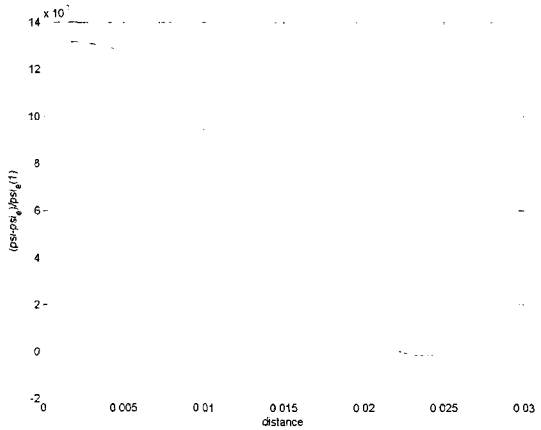

Fig. 10 Relative rotation error for applied moment

shown in Fig.1. The applied loads are $F_{zb}=5000$ N and $F_{zt}=-5000$ N. Displacement and rotation for Mode I are shown in Fig. 11. There is no x-directional displacement because only F load, which is depicted in Fig. 1, is applied. The displacement in the z-direction and rotation are shown in Figs. 12 and 13, respectively. The deformations of the top and bottom parts are symmetric because the heights of top and bottom beam are equal.

In Mode II the loads are antisymmetric and the crack tip is under Mode II condition. The applied loads for Mode II are $F_{xb}=5000$ N and $F_{xt}=-5000$ N. The x-directional displacement

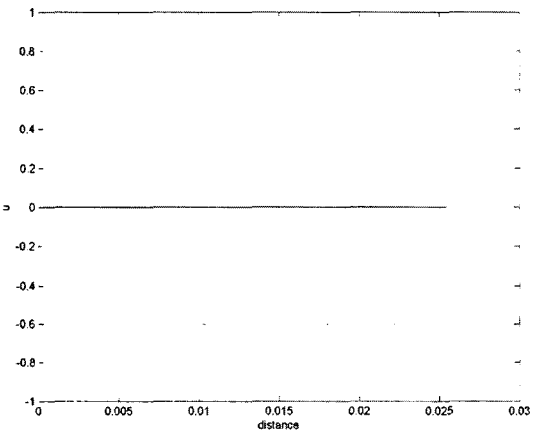

Fig. 11 x-direction displacement for Mode I (solid : top, dotted : bottom)

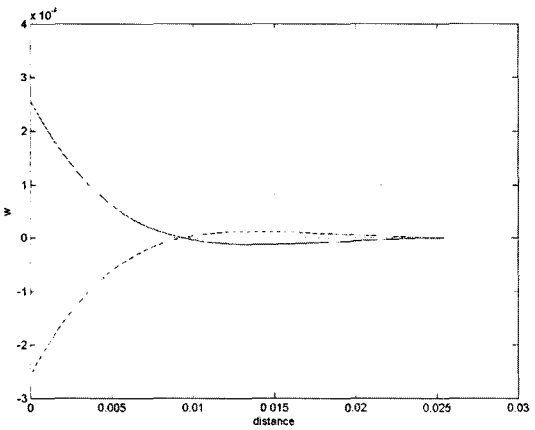

Fig. 12 z-direction displacement for Mode I (solid : top, dotted : bottom)

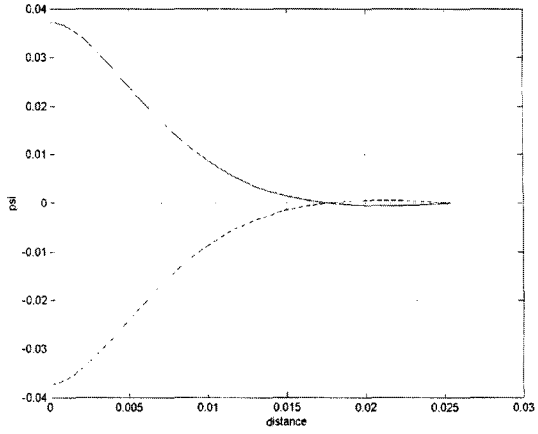

Fig. 13 Rotation for Mode I (solid : top, dotted : bottom)

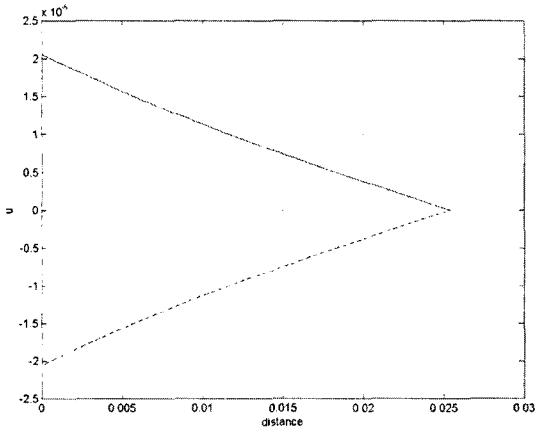

Fig. 14 x-direction displacement for Mode II (solid : top, dotted : bottom)

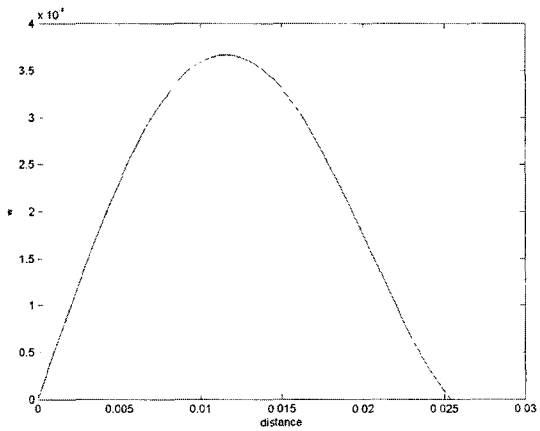

Fig. 15 z-direction displacement for Mode II (solid : top, dotted : bottom)

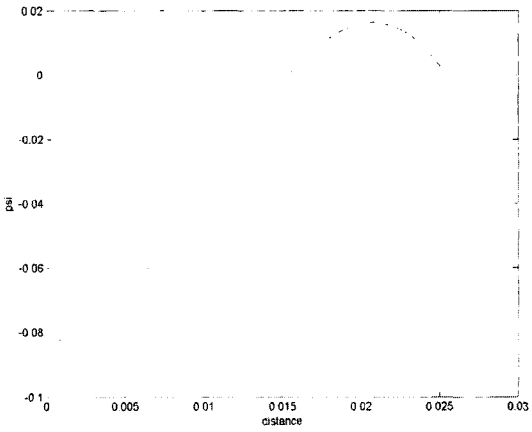

Fig. 16 Rotation for Mode II (solid : top, dotted : bottom)

almost linearly decreases with respect to x as shown in Fig. 14. However, transverse deflection and rotation are of higher order in x, and top and bottom parts show identical trend as shown in Figs. 15 and 16. The stitches have an effect on the z-direction displacements although there is only x-directional applied load.

The results for mixed mode loading, combination of Mode I and Mode II, can be obtained by superposition.

5. Conclusion

An analytical model has been developed for simulating the behavior of stitched double cantilever beam specimen under various loading conditions. For z-directional load and moment about the y-axis the numerical solutions are compared with the exact solutions. The stitched beam is considered as a finite length beam on elastic foundation when we try to find exact solutions of the problem. The derived formulation shows good accuracy when the relative error of displacement and rotation between numerical and exact solution were calculated. Thus we can use the present model with confidence in analyzing other problems involving stitched beams. The calculations have been carried out for two different load conditions. Three kinds of displacement, x- and z-directional displacements and rotation about the y-axis, are obtained for each mode. Mode I is the case where the applied load is symmetric. There is no x-directional displacement because of only z-direction load. The displacement in the z-direction and rotation are symmetrical shape because of the symmetry of the top and bottom beams.

When a positive axial load (in the $+x$ direction) is applied on the lower beam and a negative load (in the $-x$ direction) load is applied on the upper beam the condition becomes Mode II. The x-directional displacement almost linearly decreases. However, only x-directional displacement is symmetric and linear in the Mode II condition. The z-direction displacement and rotation behavior of top and bottom beam is equal in the Mode II. The results for mixed mode conditions can be obtained by superposition. The methods described in this paper can be easily extended to other loading conditions such as applied end couple. After the displacements are calculated, the forces in the stitches can be determined from Eqs. (6-8), and can be used to find the load at which the stitch will break. Calculation of energy release rate at the crack tip and estimating the bridging length etc. will be the topic of future work and they will be discussed in a sequel to this paper. The method developed in this paper will be useful in analyzing progressive damage in stitched composite beams and in estimating their apparent fracture toughness.

Acknowledgment

This work had been done during sabbatical leave at University of Florida. The authors are grateful for the support provided by Hongik University.

References

Chen, L., Ifju, P. G. and Sankar, B. V., 2001, "A Novel Double Cantilever Beam Test for Stitched Composite Laminates," *Journal of Composite Materials*, Vol. 35, No. 13, pp. 1137~1149.

Chen, L., Sankar, B. V. and Ifju, P. G., 2003, "Mixed Mode Fracture Toughness Tests for Stitched Composite Laminates," *AIAA* 2003-1874.

Choi, B. S. and Chai, Y. S., 2002, "Interfacial Crack Propagation Under Various Mode-Mixes," *KSME International Journal*, Vol. 16, No. 1, pp. 39~45. (in Korea)

Reeder, J. R. and Crews, J. H. Jr., 1992, "Redesign of the Mixed Mode Bending Delamination Test to Reduce Nonlinear Effect," *Journal of Composite Technology and Research*, pp. 12~18.

Ridards, R. and Korjakin, A., 1998, "Interlaminar Fracture Toughness of GFRP Influenced by Fiber Surface Treatment," *Journal of Composite Materials*, Vol. 32, No. 17, pp. 1528~1559.

Rugg, K. L., Cox, B. N. and Massabo, R., 2002, "Mixed Mode Delamination of Polymer Composite Laminates Reinforced Through the Thickness by z-fibers," *Composites-Part A : Applied Science and Manufacturing*, Vol. 33, No. 2, pp. 177~190.

Sankar, B. V. and Dharmapuri, S. M., 1998, "Analysis of a Stitched Double Cantilever Beam.," *Journal of Composite Materials*, Vol. 32, No. 24, pp. 2203~2225.

Sankar, B. V. and Sharma, K. S., 1995, "Effects of Through-the-thickness Stitching on Impact and Interlaminar Fracture Properties of Textile Graphite/Epoxy Laminates," *NASA CR*-195042. NASA Langley, Hampton, VA.

Song, S. H. and Lee, J. M., 2003, "Fatigue Crack Propagation Behavior in STS304 Under Mixed-Mode Loading," *KSME International Journal*, Vol. 17, No. 6, pp. 796~804. (in Korea)

Young, W. C., 1989, Roark's Formulas for Stress and Strain, Sixth Edition, McGraw-Hill Book Co., New York, p. 140.

Appendix I

The matrix form of linear equation in p:

$$\bar{A}\tilde{P}=\tilde{B}$$

where

$$\bar{A}=\begin{bmatrix}
-1 & 0 & \frac{2D}{Q} & & 0\ \frac{D}{Q}\alpha_5^2 & \frac{D}{Q}\alpha_5^2 & \frac{D}{Q}\alpha_5^2 & \frac{D}{Q}\alpha_5^2 \\
-1 & 0 & \frac{2D}{Q} & & 0\ \frac{D}{Q}r_5\alpha_5^2 & \frac{D}{Q}r_6\alpha_6^2 & \frac{D}{Q}r_7\alpha_7^2 & \frac{D}{Q}r_8\alpha_8^2 \\
0 & 1 & 0 & & 0\ \alpha_5 & \alpha_6 & \alpha_7 & \alpha_8 \\
0 & 1 & 0 & 0 & r_5\alpha_5 & r_6\alpha_6 & r_7\alpha_7 & r_8\alpha_8 \\
1 & c & c^2 & c^3 & e^{\alpha_5 c} & e^{\alpha_6 c} & e^{\alpha_7 c} & e^{\alpha_8 c} \\
1 & c & c^2 & c^3 & r_5 e^{\alpha_5 c} & r_u e^{\alpha_6 c} & r_7 e^{\alpha_7 c} & r_8 e^{\alpha_8 c} \\
-c & -\frac{1}{2}c^2 & \frac{2Dc}{Q} & -\frac{c^3}{3}\frac{3Dc^2}{Q} & -\frac{c^4}{4}\left(\frac{D}{Q}\alpha_5^2-1\right)\frac{e^{\alpha_5 c}}{\alpha_5} & \left(\frac{D}{Q}\alpha_u^2-1\right)\frac{e^{\alpha_6 c}}{\alpha_6} & \left(\frac{D}{Q}\alpha_7^2-1\right)\frac{e^{\alpha_7 c}}{\alpha_7} & \left(\frac{D}{Q}\alpha_8^2-1\right)\frac{e^{\alpha_8 c}}{\alpha_8} \\
-c & -\frac{1}{2}c & \frac{2Dc}{Q} & -\frac{c^3}{3}\frac{3Dc^2}{Q} & -\frac{c^4}{4}\left(\frac{D}{Q}\alpha_5^2-1\right)\frac{r_5 e^{\alpha_5 c}}{\alpha_5} & \left(\frac{D}{Q}\alpha_6^2-1\right)\frac{r_6 e^{\alpha_6 c}}{\alpha_6} & \left(\frac{D}{Q}\alpha_7^2-1\right)\frac{r_7 e^{\alpha_7 c}}{\alpha_7} & \left(\frac{D}{Q}\alpha_8^2-1\right)\frac{r_8 e^{\alpha_8 c}}{\alpha_8}
\end{bmatrix}$$

$$\tilde{B}=\begin{bmatrix}
\frac{F_t}{Q}-\frac{D}{Q}(\lambda_1^2 g_3+\lambda_2^2 g_4)-\frac{1}{2}\frac{h}{Q}B(c_3\lambda_1^2+c_4\lambda_2^2) \\
\frac{F_b}{Q}-\frac{D}{Q}(\lambda_1^2 h_3+\lambda_2^2 h_4)-\frac{1}{2}\frac{h}{Q}B(c_3\lambda_1^2+c_4\lambda_2^2) \\
\frac{C_t}{D}-g_3\lambda_1-g_4\lambda_2 \\
\frac{C_b}{D}-h_3\lambda_1-h_4\lambda_2 \\
-g_3 e^{\lambda_1 c}-g_4 e^{\lambda_2 c} \\
-h_3 e^{\lambda_1 c}-h_4 e^{\lambda_2 c} \\
-\left(\frac{D}{Q}\lambda_1^2-1\right)\frac{g_3}{\lambda_1}e^{\lambda_1 c}-\left(\frac{D}{Q}\lambda_2^2-1\right)\frac{g_4}{\lambda_2}e^{\lambda_2 c}-\frac{1}{2}\frac{h}{Q}B(c_3\lambda_1 e^{\lambda_1 c}+c_4\lambda_2 e^{\lambda_2 c}) \\
-\left(\frac{D}{Q}\lambda_1^2-1\right)\frac{h_3}{\lambda_1}e^{\lambda_1 c}-\left(\frac{D}{Q}\lambda_2^2-1\right)\frac{h_4}{\lambda_2}e^{\lambda_2 c}-\frac{1}{2}\frac{h}{Q}B(c_3\lambda_1 e^{\lambda_1 c}+c_4\lambda_2 e^{\lambda_2 c})
\end{bmatrix}$$

Appendix II

The analytical solutions of deflection and rotation for z-directional load F are expressed as follows :

$$w_F = y_{AF}\cosh\beta x\cos\beta x + \frac{\psi_{AF}}{2\beta}(\cosh\beta x\sin\beta x+\sinh\beta x\cos\beta x) - \frac{F}{4EI\beta^3}(\cosh\beta x\sin\beta x-\sinh\beta x\cos\beta x)$$

$$\psi_F = \psi_{AF}\cosh\beta x\cos\beta x - y_{AF}\beta(\cosh\beta x\sin\beta x-\sinh\beta x\cos\beta x) - \frac{F}{4EI\beta^3}\sinh\beta x\sin\beta x$$

where

$$y_{AF}=\frac{F}{2EI\beta^3}\frac{C_1C_4-C_2C_3}{2+C_{11}}$$

$$\psi_{AF}=\frac{F}{2EI\beta^3}\frac{2C_1C_3+C_4C_4}{2+C_{11}}$$

The analytical solutions of deflection and rotation for applied moment M are expressed as follows :

$$w_M = y_{AF}\cosh\beta x\cos\beta x + \frac{\psi_{AM}}{2\beta}(\cosh\beta x\sin\beta x+\sinh\beta x\cos\beta x) + \frac{M}{2EI\beta^2}\sinh\beta x\sin\beta x$$

$$\psi_M = \psi_{AM}\cosh\beta x\cos\beta x - y_{AM}\beta(\cosh\beta x\sin\beta x-\sinh\beta x\cos\beta x) + \frac{M}{2EI\beta}(\cosh\beta x\sin\beta x+\sinh\beta x\cos\beta x)$$

where

$$y_{AM}=\frac{M}{2EI\beta^2}\frac{2C_1C_3-C_2C_2}{2+C_{11}}$$

$$\psi_{AM}=-\frac{M}{EI\beta}\frac{C_1C_2+C_4C_3}{2+C_{11}}$$

$$\beta=\left(\frac{b_0k_0}{4EI}\right)^{1/4}$$

$$C_1=\cosh\beta l\cos\beta l$$
$$C_2=\cosh\beta l\sin\beta l+\sinh\beta l\cos\beta l$$
$$C_3=\sinh\beta l\sin\beta l$$
$$C_4=\cosh\beta l\sin\beta l-\sinh\beta l\cos\beta l$$
$$C_{11}=\sinh^2\beta l-\sin^2\beta l$$